# High-Temperature Degradation Mechanism of $Cu(In,Ga)Se_2$-Based Thin Film Solar Cells



2008 Appl. Phys. Express 1 075002

(http://iopscience.iop.org/1882-0786/1/7/075002)

# High-Temperature Degradation Mechanism of Cu(In,Ga)$Se_2$-Based Thin Film Solar Cells

Shunsuke Kijima and Tokio Nakada

*Department of Electrical Engineering and Electronics, Aoyama Gakuin University, 5-10-1 Sagamihara, Kanagawa 229-8558, Japan*

Received March 11, 2008; accepted May 30, 2008; published online June 27, 2008

The degradation mechanism of Cu(In,Ga)$Se_2$ (CIGS) thin film solar cells under high-temperatures conditions has been investigated. CIGS thin film solar cells were heated at temperatures ranging from 100 to 450 °C in a vacuum for 30 min. It was found that the CIGS devices with chemical bath deposited (CBD)–CdS and CBD–ZnS(O,OH) buffer layers were stable below 320 and 350 °C, respectively. These results suggest that CIGS devices possess high heat-resistance enough for practical usage. Secondary ion mass spectrometer (SIMS) and electron beam induced current (EBIC) analyses revealed that the main cause for the degradation of CIGS devices at high temperatures is attributable to a shift of the space charge region (SCR) toward the Mo back contact due to excess diffusion of Cd into CIGS absorber layer.


DOI: 10.1143/APEX.1.075002

In recent years, remarkable progress has been made on Cu(In,Ga)$Se_2$ (CIGS)-based thin film solar cells and modules. In fact, CIGS thin film solar cells with efficiencies of 19.9[1] and 18.6%[2] have been achieved using chemical bath deposited (CBD)–CdS and CBD–ZnS(O,OH) buffer layers, respectively. Large-scale modules with over 13% efficiency have been reported by several industries.[3–5] CIGS thin film solar cells have also attracted attention for use in space applications because of their excellent radiation hardness.[6] To date, however, few publications on the degradation mechanism of CIGS devices in high-temperature conditions have been reported[7] although this issue is very important for practical usage of modules. In this paper, we describe the degradation mechanism of CIGS thin film solar cells with CBD–CdS and CBD–ZnS(O,OH) buffer layers, and discuss the origins of the degradation of cell performance at high temperatures.

CIGS thin film solar cells with the structure ZnO:Al/ZnO/[CdS or ZnS(O,OH)]/CIGS/Mo/SLG (soda lime glass) structures were fabricated. Approximately 2.5-μm-thick CIGS thin films were deposited on SLG substrates by the three-stage process. The average film composition was measured using inductively-coupled plasma spectroscopy (ICP). The Ga/(In + Ga) and Cu/(In + Ga) atomic ratios were maintained at the values 0.28 and 0.88, respectively, by controlling the source temperatures during CIGS deposition. CBD–CdS buffer layers were then deposited onto the CIGS layers using $CdSO_4$ (0.16 M)–ammonia (7.5 M)–thiourea (0.6 M) aqueous solutions at 80 °C. 60-nm-thick non-doped ZnO and 600-nm-thick ZnO:Al (2 wt % $Al_2O_3$-doped ZnO) thin films were deposited at room temperature by rf sputtering. The CIGS film was then cut into nine pieces after completing fabrication of the solar cell structure. A ZnS(O,OH) buffer layer was also deposited on the CIGS absorber layers using $ZnSO_4$ (0.16 M)–ammonia (7.5 M)–thiourea (0.6 M) aqueous solutions at 80 °C with ultrasonic excitation.[8] The ZnS(O,OH)/CIGS/Mo/SLG device was then heated at 200 °C to fabricate a p–n buried junction.[9] 6-nm-thick non-doped ZnO and 600-nm-thick ZnO:Al thin films were then deposited onto the buffer layers. The CIGS thin film solar cells were placed in a vacuum chamber evacuated to $5 \times 10^{-6}$ Pa, and were heated at temperatures ranging from 100 to 400 °C for 30 min. Current–voltage ($J$–$V$) characteristics were measured before and after heating by means of a solar simulator calibrated using a Si standard cell under AM 1.5, 100 mW/cm$^2$ illumination at 24 °C.

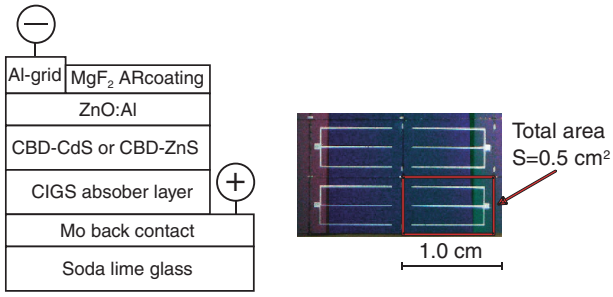


**Fig. 1.** Cell structure (a) and top view photograph (b) of a CIGS solar cell.

Figure 1 shows the cell structure and a top view photograph of the CIGS solar cell used in this experiment. The deviations in each cell parameter between nine as-fabricated devices were within ±1.4, ±4.6, ±2.3, and ±3.5% for open-circuit-voltage ($V_{oc}$), short-circuit-current ($J_{sc}$), fill factor (FF), and total-area efficiency, respectively. Figure 2 shows the temperature dependence of the basic cell parameters for CIGS thin film solar cells. As can be seen in this figure, the CIGS device was stable below 320 °C, although $J_{sc}$ and efficiency decreased slightly in this temperature range. The upper temperature limit of 320 °C is high enough for practical usage of CIGS solar cells and modules. The cell efficiency deteriorated above 340 °C due to a decrease in $V_{oc}$ and FF. In contrast, the $J_{sc}$ value was stable to 360 °C, and decreased for temperatures above 400 °C.

Figure 3 shows the temperature dependence of the spectral response curves for the CIGS devices shown in Fig. 2. As can be seen in this figure, almost the same spectral response curves were observed for devices heated at temperatures below 360 °C. In contrast, the quantum efficiency (QE) for a device heated to 400 °C decreased over a wide wavelength range. This behavior agrees well with the temperature dependence of the $J_{sc}$ values shown in Fig. 2. The cause for the high stability of $J_{sc}$ is not fully understood at present.

In shed light on the degradation mechanism, we have investigated changes in junction location using electron beam induced current (EBIC)[10,11] measurements in a high-resolution field emission scanning electron microscope (FE-SEM; HITACHI S4800). EBIC images and line-scan profiles of CIGS solar cells before and after heating in vacuum are shown in Fig. 4. The EBIC profiles have been superimposed on SEM topographic images for clarity. The red area of the

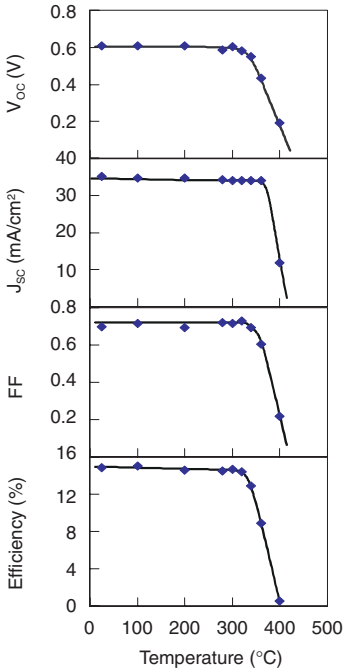


**Fig. 2.** The temperature dependence of the basic solar cell parameters for CdS/CIGS thin film solar cells.

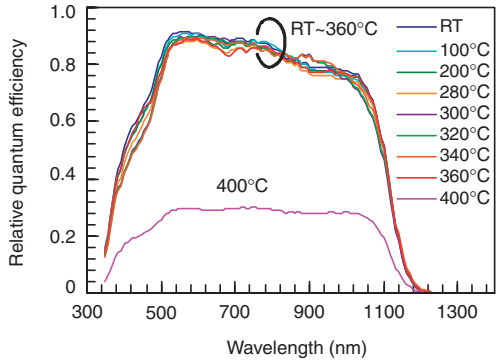


**Fig. 3.** The temperature dependence of the spectral response curves of CIGS devices shown in Fig. 2.

EBIC image indicates a photo-generated region, that is a space-charge region (SCR) plus the minority carrier diffusion length. It is clear that the SCR is present near the CdS/CIGS hetero-interface for the as-fabricated solar cell [Fig. 4(a)]. The SCR of the same device after heating at 280 °C widened slightly, and it spanned the entire CIGS absorber layer after heating at 360 °C. The widening of the SCR implies a decrease in carrier concentration, resulting in a lowered built-in potential, and hence a decreased $V_{oc}$ value as shown in Fig. 2. The SCR moved completely to near the Mo back contact and the peak height significantly decreased at 400 °C as shown Fig. 4(d). The SCR image suggests a widened n-type region throughout the CIGS absorber, resulting in a decrease in blue response as seen in Fig. 3.

In order to reveal the cause for the shift of the SCR after heating, we have carried out SIMS analysis of the CdS/CIGS interface. Prior to the SIMS analysis Ar etching was carried out to thin the glass substrates. SIMS analysis of the CdS/CIGS interface was performed using Cs ions from the glass substrate-side to prevent the mixing or knocking of Cd

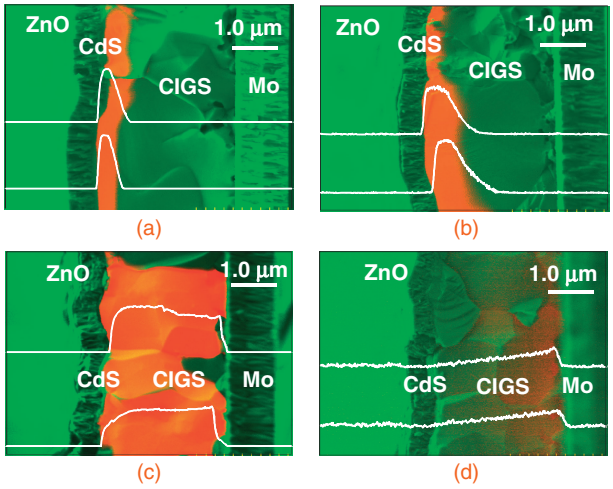


**Fig. 4.** EBIC images and line-scan profiles of the CdS/CIGS solar cells (a) before and after heating at (b) 280, (c) 360, and (d) 400 °C in a vacuum.

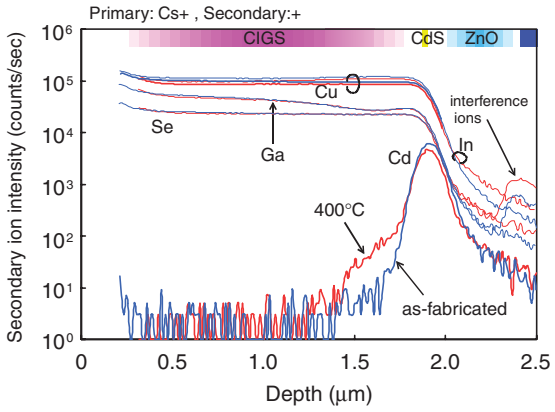


**Fig. 5.** SIMS depth profiling of Cd at the CdS/CIGS interface before and after heating at 400 °C in a vacuum.

into CIGS. Figure 5 shows a secondary ion mass spectrometer (SIMS) analysis of the CdS/CIGS interface before and after heating at 400 °C. It is clear from the figure that the Cd has diffused into the CIGS layer after heating at 400 °C. The apparent diffusion length of Cd was approximately 0.5 μm within the detection limit of SIMS analysis. However, it should be noted that a small amount of Cd may diffuse into deeper regions of the CIGS layer than observed in Fig. 5. This suggests the substitution of $Cd^{2+}$ for $Cu^{+}$ and/or Cu vacancies (acceptors). This is followed by the increase in donor minus acceptor concentration. The diffusion of Cd into the CIGS layer may therefore result in the formation of a buried p–n junction in the CIGS-based absorber layer.[12–14)]

Based on the EBIC and SIMS analyses mentioned above, it can be concluded that the deterioration in cell performance after heating is attributable to the excess diffusion of Cd into the CIGS absorber layer.

We also have carried out similar experiments using a ZnS(O,OH)/CIGS structure. Figure 6 shows the temperature dependence of the solar cell parameters for ZnS(O,OH)/CIGS devices. As can be seen in the figure, the ZnS(O,OH)/CIGS device was stable below 350 °C, a value higher than that of cells fabricated using a CdS buffer layers and high

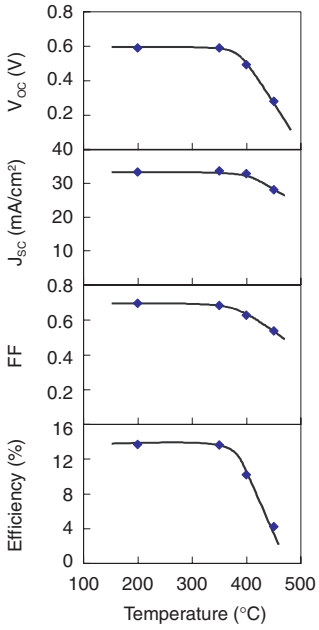


**Fig. 6.** The temperature dependence of basic solar cell parameters for ZnS(O,OH)/CIGS devices.

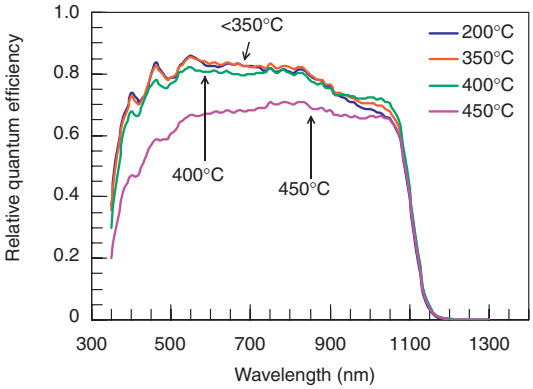


**Fig. 7.** The temperature dependence of the spectral response curves for ZnS(O,OH)/CIGS devices.

enough for practical usage of the device. The cell efficiency deteriorated for temperatures above 400 °C due to a decrease in $V_{oc}$ and FF. In contrast the $J_{sc}$ value was stable to 400 °C. This behavior is nearly the same as that of the CdS/CIGS devices mentioned above.

Figure 7 shows the temperature dependence of the spectral response curves of ZnS(O,OH)/CIGS devices. Nearly the same spectral response curves were observed for the devices heated to a maximum temperature below 350 °C. The QE was found to decrease at short wavelengths at temperatures above 450 °C. We have also carried out EBIC analysis to understand the temperature dependence of this device. Figure 8 shows EBIC images and line-scan profiles of ZnS(O,OH)/CIGS solar cells before and after heating at 450 °C in a vacuum. It is clear that the SCR is present near the CdS/CIGS hetero-interface for an as-fabricated solar cell and moves back toward the Mo back contact after heating. We have also confirmed by SIMS analysis that Zn atoms diffused into CIGS from the ZnS(O,OH) buffer layer after heating. These results suggest

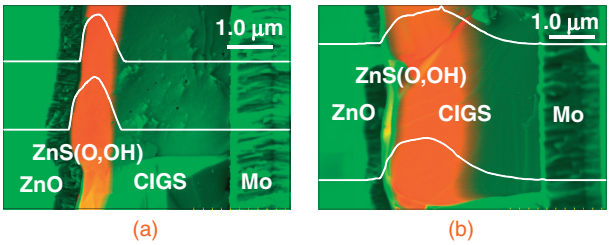


**Fig. 8.** EBIC images and line-scan profiles of ZnS(O,OH)/CIGS solar cells (a) air-annealing at 200 °C for 10 min and (b) heated at 450 °C in a vacuum for 30 min after the same air-annealing process.

that changes in the p–n junction due to excess diffusion of Zn after heating lead to deterioration in cell performance.

In conclusion, we found that CdS/CIGS and ZnS(O,OH)/CIGS devices are stable below 320 °C and 350 °C, respectively. These results suggest that CIGS devices possess high heat-resistance for practical usage. It was also found that the main cause for the deterioration of CIGS devices under high temperatures is attributable to a shift in the location of the SCR toward the Mo back contact due to the excess diffusion of Cd or Zn into the CIGS absorber layer.

**Acknowledgment** This work was partially supported by New Energy and Industrial Technology Development Organization (NEDO) as a part of "Investigation for innovative photovoltaic (PV) technology" project Part-II (FY2004-2005).

1) I. Repins, M. A. Contreras, B. Egaas, C. DeHart, J. Scharf, C. L. Perkins, B. To, and R. Noufi: Prog. Photovoltaics **16** (2008) 235.
2) M. A. Contreras, T. Nakada, M. Hongo, A. O. Pudov, and J. R. Sites: Proc. 3rd World Conf. Photovoltaic Energy Conversion, Osaka, 2003, p. 570.
3) M. Powalla, B. Dimmler, R. Schaeffer, G. Voorwinden, U. Stein, H.-D. Mohring, F. Kessler, and D. Hariskos: Proc. 19th European Photovoltaic Solar Energy Conf., Paris, 2005, p. 1663.
4) V. Probst, J. Palm, S. Visbeck, T. Niesen, R. Tolle, A. Lerchenberger, M. Wendl, H. Vogh, H. Calwe, W. Stette, and F. Karg: Tech. Dig. 14th Int. Photovoltaic Science and Engineering Conf., Bangkok, 2004, p. 663.
5) K. Kushiya, T. Tanaka, Y. Nagoya, M. Tachiyuki, and M. Akema: Proc. 19th European Photovoltaic Solar Energy Conf., Paris, 2005, p. 1672.
6) S. Kawakita, M. Imaizumi, M. Yamaguchi, K. Kushiya, T. Ohshima, H. Ito, and S. Matsuda: Proc. 2nd World Conf. Photovoltaic Energy Conversion, Vienna, 1998, p. 3568.
7) S. Kijima and T. Nakada: Tech. Dig. 15th Photovoltaic Solar Energy Conf., 2005, p. 903.
8) A. Ichiboshi, M. Hongo, T. Akamine, T. Dobashi, and T. Nakada: Sol. Energy Mater. Sol. Cells **90** (2006) 3130.
9) T. Nakada and M. Mizutani: Proc. 28th IEEE Photovoltaic Solar Energy Conf., Anchorage, 2000, p. 529.
10) S. Ishizuka, K. Sakurai, A. Yamada, K. Matsubara, P. Fons, T. Baba, Y. Kimura, S. Nakamura, H. Nakanishi, and S. Niki: Tech. Dig. 14th Int. Photovoltaic Science and Engineering Conf., Bangkok, 2004, p. 527.
11) S. Ishizuka, K. Sakurai, K. Matsubara, A. Yamada, M. Yonemura, S. Kuwamori, S. Nakamura, H. Nakanishi, and S. Niki: Mater. Res. Soc. Symp. Proc. **865** (2005) 265.
12) T. Nakada and A. Kunioka: Appl. Phys. Lett. **74** (1999) 2444.
13) K. Ramanathan, R. N. Bhattacharya, J. Granata, J. Webb, D. Nieles, M. A. Contreras, H. Wiesner, F. S. Hasoon, and R. Noufi: Proc. 26th IEEE Potovoltaic Specialists Conf., 1997, p. 319.
14) T. Wada, S. Hayashi, Y. Hashimoto, S. Nishiwaki, T. Sato, T. Negami, and M. Nishitani: Proc. 2nd World Conf. Photovoltaic Energy Conversion, Vienna, 1998, p. 403.